The Influence of Vibrations on the Electromechanical Impedance Method Applied to Square Thin Plates

Cristian RUGINA*
Institute of Solid Mechanics of the Romanian Academy, str.C-tin Mille, no. 15, sector 1, 010141, Bucharest, Romania, rugina.cristian@imsar.ro
INCAS National Institute for Aerospace Research „Elie Carafoli", Iuliu Maniu 220, sector 6, 061126, Bucharest, Romania, rugina.cristian@incas.ro

Dan DUMITRIU
Institute of Solid Mechanics of the Romanian Academy, str.C-tin Mille, no. 15, sector 1, 010141, Bucharest, Romania, dan.dumitriu@imsar.ro

Ioan URSU
INCAS National Institute for Aerospace Research „Elie Carafoli", Iuliu Maniu 220, Sector 6, 061126, Bucharest, Romania, ursu.ioan@incas.ro

Mihai TUDOSE
INCAS National Institute for Aerospace Research „Elie Carafoli", Iuliu Maniu 220, sector 6, 061126, Bucharest, Romania, tudose.mihai@incas.ro

* Author to whom correspondence should be addressed

Abstract: The paper studies the influence of external vibrations on the electromechanical impedance signature of thin square aluminum plates. The plate has bonded on it two piezoelectric elements: one bonded in the center of the plate used for electromechanical impedance and another, on the corner, for generating small external vibrations. The spectrum frequencies of external vibrations were considered to be in the medium and high frequency range, with different levels of amplitudes. The plate is hung by a hook, and free boundary conditions at the plate's edge are therefore considered. Comparisons of different bonding adhesives of the piezoelectric elements, permanent and temporary, are experimentally done. Comparisons of experimental electromechanical impedance measurements with and without vibrations at different fixed frequencies are presented to evaluate their effects. Theoretical electromechanical impedance signature calculated by three methods, integration method, correlation method, and Discrete Fourier Transform, was compared with the experimental data, on a simulated signal similar to the ones acquired by impedance analyzers. Comparisons of experimental data and numerical finite-element results for the electromechanical impedance signature are also made.

Keywords: Structural Health Monitoring, SHM, Electromechanical Impedance Method, EMI, EMIS, Vibrations

1. INTRODUCTION

The active and passive ultrasonic SHM systems are becoming more and more used, especially on aerospace vehicles with thin plate structures [1-6]. The active ultrasonic SHM sensing techniques are based on two different approaches: transient guided waves and standing waves [1]. In such SHM processes, a piezoelectric wafer active sensor (PWAS) is required to generate elastic waves. These travel along the mechanical structure, are reflected by different structural abnormalities, i.e., cracks, corrosions, delamination, and others, or from the boundary edges, and then are recaptured by the same sensor in a pulse-echo configuration or by other sensors of same or different type, even passive sensors, in pitch-catch configuration [1]; this is the so-called method of tuned Lamb waves. If the structural damage or boundary edges are in the immediate vicinity of the active sensor, their reflections overlap with the incident transient wave, making interpretation impossible. This drawback can be overcome by using the ultrasonic standing waves, in the so-called electromechanical impedance spectroscopy method (EMI) (also known as EMIS or E/M method). By sweeping the frequency of the input signals to PWAS, some changes appear in the impedance measured by an Impedance Analyzer connected to the PWAS terminals.

By monitoring the changes in the real part of the impedance function, which is most sensitive to structural changes, one can evaluate the integrity of the host structure [1-4]. The EMI method was proven to be effective experimentally, as well as analytical and numerical finite element method (FEM) simulations. For circular sample plates, an analytical solution exists [1-4]. For complicated geometries, only numerical FEM simulations can be done. An extensive review of the EMI method, including experimental, analytical, and numerical aspects, was conducted in [7].

Usually, the EMI method is studied on static plates that do not consider the structural perturbations caused by the external sources of excitation. In practice, all structures are subjected to different kinds of mechanical perturbations. Most of these mechanical perturbations can be translated to different vibration levels of the structures, which can influence the results of SHM by causing changes in the EMI signatures. The changes in EMI signatures due to the external vibrations and those of structural damage must be differentiated so that the correct information on structural health can be obtained.

The effect of external vibrations on the EMI signature has been studied. An analytical solution on the EMI signature on a uniform beam with simply supported boundary conditions subjected to extensional vibration was studied in [8]. In [9], a custom EMI analyzer was used to study the effect of external vibrations on the EMI signature on an Aluminum strip with two piezoelectric transducers bonded on it, one for the EMI method and another for generating the external vibration with a chirp and white noise signal simulating vibrations of rotating devices.

This paper studies the effect of vibration on the EMI signature on a square thin plate actuated with circular PWAS for generating vibrations. The plate has bonded to it two PWAS: one bonded in the center of the plate, used for EMI analysis, and another on the corner, used to generate small external vibrations across different spectral ranges: acoustic (medium) and ultrasonic (high) frequencies. The corner PWAS connected to a signal generator is used as a vibration generator, outside the vibration generated by the EMI PWAS. The study uses external vibration excitations with a single frequency and a combination of two frequencies, which can be easily applied with a two-channel signal generator, different from chirp and white noise used in [9], and the conclusions can be extended, as every signal is a combination of multiple frequencies.

Two types of bonding materials were considered: permanent bonding with epoxy and temporary bonding with tar, and comparisons of their EMI signatures were made. Comparisons of the experimental and computed EMI signature was also done, in the case of no external vibrations, to confirm the validity of the measurements.

As it was experimentally observed that external vibrations do influence significantly the EMI signature, a theoretical study was done to explain the errors in the measured data when the external vibration frequencies are in-band with the EMI spectrum. The theoretical study consists of applying three methods for the calculation of the EMI signature: the Integration method, the Correlation method, and the Discrete Fourier Transform method, explained in [10], on simulated mathematically generated and discretized sinusoidal signals similar to the ones acquired by our impedance analyzer, in terms of sampling frequency and number of samples.

2. THEORETICAL METHODS

In this paper, we analyze the EMI method on thin square plates subjected to external vibrations, both experimentally and numerically.

a) The experimental method

The EMI method consists of measuring the voltage, current, and phase shift across the piezoelectric disks using an electrical resistive component and an electrical reactive component.

$$V = |V| e^{j(\omega t - \phi_V)}, \; I = |I| e^{j(\omega t - \phi_I)} \tag{1}$$

By sweeping the frequency over a chosen range, a signature of the disks' electromechanical impedance can be obtained. The electrical impedance and admittance are defined as:

$$Z = \frac{\tilde{V}}{\tilde{I}} = \left|\frac{\tilde{V}}{\tilde{I}}\right| e^{j(\phi_V - \phi_I)}, \; Y = \frac{1}{Z} \tag{2}$$

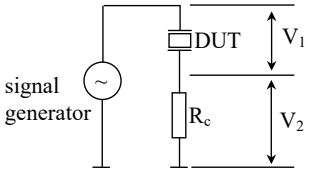

DUT – Device under testing: Piezoelectric element bonded to a mechanical structure

R_c - calibrated resistor

Figure 1. Impedance measurement principle

The electric impedance and admittance can be written as:

$$Z = |Z| e^{j\phi}, \; Z = R + jX \tag{3}$$
$$Y = |Y| e^{j\varphi}, \; Y = G + jB$$

with $|Z|$ the modulus of Z, ϕ the phase shift, R the resistance, X the reactance, $|Y|$ the modulus of Y, φ the phase shift, G the conductance, B the susceptance.

Practically, to measure the amplitude of V and I and the phase shift between them, the impedance analyzer uses a calibrated resistor to measure the voltages V_1 and V_2 as in Figure 1. The calibrated resistor has no reactive part, so the voltage and the current that pass through it do not have a phase shift. The impedance is calculated as:

$$Z = \frac{\tilde{V}_1}{\tilde{I}} = \frac{\tilde{V}_1}{\tilde{V}_2} R_c \tag{4}$$

In our measurements, we used two impedance analyzers, HP41294 and Analog Discovery 2 (AD2), which can be set to measure ($|Z|, \phi$) or (R, X) or ($|Y|, \varphi$) or (G, B), all of the pairs being equivalent, deducible from one another. In piezoelectric devices, the peaks of the admittance coincide with the mechanical resonance, while the impedance peaks coincide with the mechanical antiresonance. The (R, X) pair is the most used in practical applications and is the one we chose.

The algorithms used by impedance analyzers for determining the impedance modulus $|Z|$ and the phase shift ϕ are commercial secrets. However, three methods of determining the modulus of impedance and phase shift are available [10], and are presented shortly here:

a.1. *The Integration method*

This method, studied and explained in [10], is based on the calculations of the first coefficient of the complex Fourier series expansion of a signal.

The method considers a signal $x(t) = A\sin(\omega t + \varphi)$ that is multiplied by a sine signal and by a cosine signal, respectively, and then integrated over a time duration T. If T is the period of the signal $x(t)$, the outputs will be the real part $A\cos(\varphi)$, and the imaginary part $A\sin(\varphi)$, of this harmonic voltage $x(t)$:

$$A\cos(\varphi) = \frac{2}{T}\int_0^T A\sin(\omega t + \varphi)\sin(\omega t)\,dt$$

$$A\sin(\varphi) = \frac{2}{T}\int_0^T A\sin(\omega t + \varphi)\cos(\omega t)\,dt \tag{5}$$

a.2. *The Correlation method*

This method, also studied and explained in [10], is based on the correlation of two signals of the form:

$$x(t) = A\sin(\omega t + \varphi_0) + N_x(t) \tag{6}$$

where A is the amplitude of the signal $x(t)$, B is the amplitude of the signal $y(t)$, $N_x(t)$ is the noise of the signal $x(t)$, $N_y(t)$ is the noise of the signal $y(t)$, φ_0 is the initial phase of the signal $x(t)$, φ_1 is the amplitude of the signal $y(t)$.

By this method, thoroughly explained in [10], considering the noise of the signals uncorrelated, the phase shift $\varphi = \varphi_1 - \varphi_0$ and the amplitudes A and B of the signals can be calculated by:

$$\varphi = \arccos\frac{R_{xy}(0)}{\sqrt{R_{xx}(0)\cdot R_{yy}(0)}}$$

$$A = \sqrt{2R_{xx}(0)},\ B = \sqrt{2R_{yy}(0)} \tag{7}$$

where $R_{xx}(0)$, $R_{yy}(0)$, $R_{xy}(0)$ are:

$$R_{xy}(0) = \frac{1}{N}\sum_{n=0}^{N-1} x(n)y(n)$$

$$R_{xx}(0) = \frac{1}{N}\sum_{n=0}^{N-1} x^2(n) \tag{8}$$

$$R_{yy}(0) = \frac{1}{N}\sum_{n=0}^{N-1} y^2(n)$$

a.3. *The Discrete Fourier Transform method*

This method, studied and thoroughly explained in [10], is based on the DFT of a signal $x(t) = A\sin(2\pi ft + \varphi)$, with amplitude A, frequency f and phase shift φ. After sampling the signal $x(t)$ is $x(n)$:

$$x(n) = A\sin(2\pi fnT_s + \varphi) = A\sin\left(2\pi n\frac{f}{f_s} + \varphi\right)$$
$$= A\sin\left(2\pi q\frac{n}{N} + \varphi\right), \qquad n = 0,1,2,\ldots,N-1 \tag{9}$$

where $q = fN/f_s$, N is the number of samples, f_s is the sampling frequency, $T_s = 1/f_s$ is the sampling time.

The Discrete Fourier Transform of the signal $x(n)$ is given by [10]:

$$X(k) = \sum_{n=0}^{N-1} x(n)e^{-j(2\pi/N)kn} =$$
$$= A\frac{j}{2}e^{j\varphi}\sum_{n}^{N-1}\left(e^{-j2\pi(q+k)n/N} - e^{-j2\pi(q-k)n/N}\right) \tag{10}$$

with $k = 0,1,...,N-1$ $j = \sqrt{-1}$

As the signal is a harmonic of frequency f, it has only one spectrum component. As explained in [10] for:

$$k \neq q, N-q; \quad X(k) = 0$$

$$k = q, N-q; \quad X(k) = \frac{A}{2} N \sin\varphi - j\frac{A}{2} N \cos\varphi \quad (11)$$

b) The computational methods

The numerical model used in this paper is the finite element method, implemented in the software Comsol 6.2. A coupled field frequency analysis based on piezoelectric constitutive equations that include structural losses has been taken into consideration, for the stress-charge formulation, with the following symbol notation, according to Comsol 6.2 User Guide:

$$\sigma = \tilde{c}^E \varepsilon - \tilde{e} E$$
$$D = \tilde{e}\varepsilon + \varepsilon^0 \tilde{\varepsilon}^r E \quad (12)$$

where σ denotes the stress matrix, ε denotes strains matrix, D denotes electric charge matrix, $\tilde{c}_E$ denotes the elasticity matrix, $\tilde{e}$ denotes the piezoelectric coupling matrix, $\tilde{\varepsilon}_r$ the relative permittivity matrix. In Comsol Multiphysics, the ~ symbol denotes complex values where the imaginary part defines the dissipative function of the material: $\tilde{X} = X(1 \pm j\eta_X)$ where $\eta_X = imag(\tilde{X}) / real(\tilde{X})$ is the loss factor.

The piezoceramic materials belong to the hexagonal class symmetry [11], and have compliance, piezoelectric coupling, and relative permittivity matrices in the stress-charge form (eq. 12):

$$c_E = \begin{pmatrix} c_{11} & c_{12} & c_{13} & 0 & 0 & 0 \\ c_{12} & c_{11} & c_{13} & 0 & 0 & 0 \\ c_{13} & c_{13} & c_{33} & 0 & 0 & 0 \\ 0 & 0 & 0 & c_{55} & 0 & 0 \\ 0 & 0 & 0 & 0 & c_{55} & 0 \\ 0 & 0 & 0 & 0 & 0 & c_{66} \end{pmatrix} [GPa]$$

$$c_{66} = (c_{11} - c_{12})/2$$

$$e = \begin{pmatrix} 0 & 0 & 0 & 0 & e_{15} & 0 \\ 0 & 0 & 0 & e_{15} & 0 & 0 \\ e_{31} & e_{31} & e_{33} & 0 & 0 & 0 \end{pmatrix} [C/m^2] \quad (13)$$

$$\varepsilon_r = \begin{pmatrix} \varepsilon_{11} & 0 & 0 \\ 0 & \varepsilon_{22} & 0 \\ 0 & 0 & \varepsilon_{33} \end{pmatrix}$$

3. EXPERIMENTAL SETUP

(a)

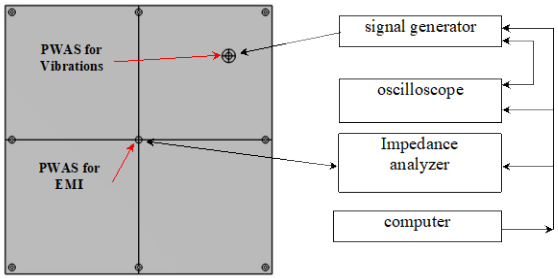

(b)

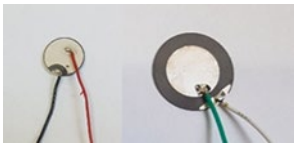

(c)

Figure 2. Experimental setup (a), block diagram (b), PWAS types used (c).

The experimental setup is presented in Figure 2.a and Figure 2.b. The EMI method is studied on Aluminum square plates with a PWAS bonded on the center of the plate and a PWAS bonded near a corner of the plate for generating vibrations. The PWAS types used are presented in Figure 2.c. The PWAS used to generate vibrations external to the EMI method is connected to a Keysight 33520 signal generator with a maximum voltage of 10Vpp and dual-channel capabilities. A Keysight DSOX4054 oscilloscope is used to acquire both the voltage on the PWAS that generates external vibrations and the voltage on the PWAS for EMI, in order to evaluate the level of external vibrations. The computer commands all the processes of data acquisition and storage. The plate is mounted in suspended position on one of the holes for free boundary conditions at the plate's edges, making it easier to model in FEM (Figure 2.a).

A comparison between EMI experimental measurements on plates with different types of bonding adhesives of the PWAS. A permanent bonding with an epoxy adhesive and a temporary adhesive with tar were considered. The permanent bonding is better at all temperatures, including high

temperatures (about maximum 260°C), but debonding the PWAS is impossible, so many more samples are needed for a comparative study on specific geometries. The temporary bonding with tar adhesive is good only for room temperature. The sensor and plate are locally heated around 120 °C, far from the Curie depolarization temperature point of about 300 °C, and cooled down to room temperature, when the tar changes phase from liquid to solid state. Debonding is done in reverse. A comparison of experimental EMI signatures with permanent and temporary adhesives (Figure 3) reveals that the permanent bonding produces higher amplitude peaks, but the positions of these peaks are almost the same. We used, in this study, only the setup with temporary bonding to have a reusable plate and PWASs.

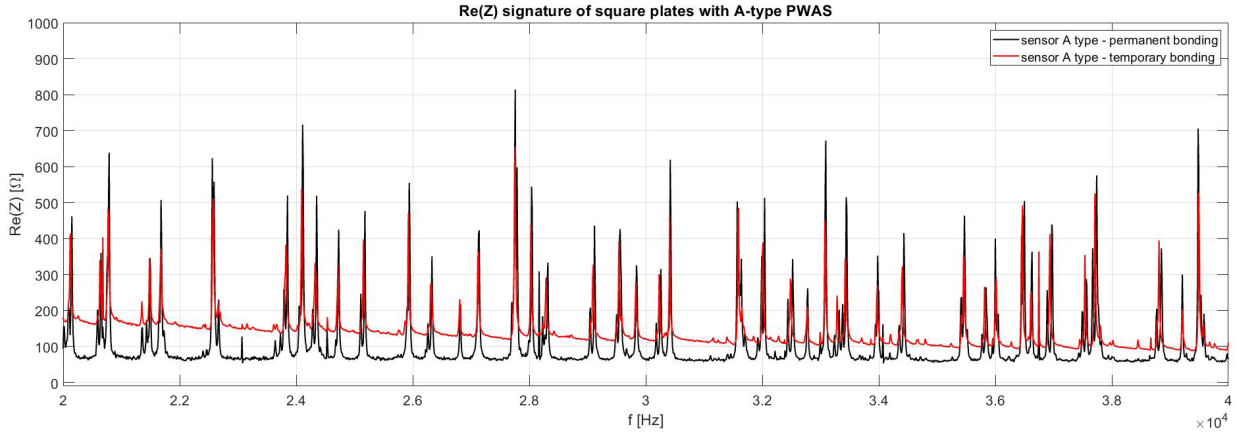

Figure 3. Impedance signature Re(Z) on square plates with both permanent and temporary bonding in the frequency range of 20kHz-40kHz.

4. RESULTS AND DISCUSSIONS

In a first step, a comparison between experimental and numerical results has been done, as an analytical solution for square plates does not exist, unlike circular plates [1-4].

The material of the PWAS was taken as PZT5A, that belong to the hexagonal class symmetry, which has compliance, piezoelectric coupling, and relative permittivity matrices in the stress-charge form (eq.13):

$$c_{11}^E = c_{22}^E = 120.35\,[GPa], c_{12}^E = 75.18\,[GPa],$$
$$c_{13}^E = c_{23}^E = 75.09\,[GPa],\ c_{33}^E = 110.86\,[GPa],$$
$$c_{44}^E = c_{55}^E = 21.05\,[GPa], c_{66}^E = 22.57\,[GPa],$$
$$e_{31} = e_{32} = -5.35\,[C/m^2], e_{33} = 15.78\,[C/m^2],$$
$$e_{15} = 12.29\,[C/m^2],\ \varepsilon_{11}^r = \varepsilon_{22}^r = 919.1,\ \varepsilon_{33}^r = 826.6.$$

The mechanical and piezoelectric structural losses for the PWAS were neglected. However, the dielectric losses of 1.9% given by the manufacturer were taken into consideration. The mass density of the piezoceramic material was considered $\rho = 7750\,[kg/m^3]$. The properties of the A7075 aluminium plate were taken:

$$E = 71.14\,[GPa],\ \rho = 2720\,[kg/m^3], \nu = 0.3312.$$

The adhesive layer between the plate and the PWAS was neglected, as shown previously in [3] that the thickness of the adhesive layer influences only the amplitude of the resonance peaks, not significantly the peak's position.

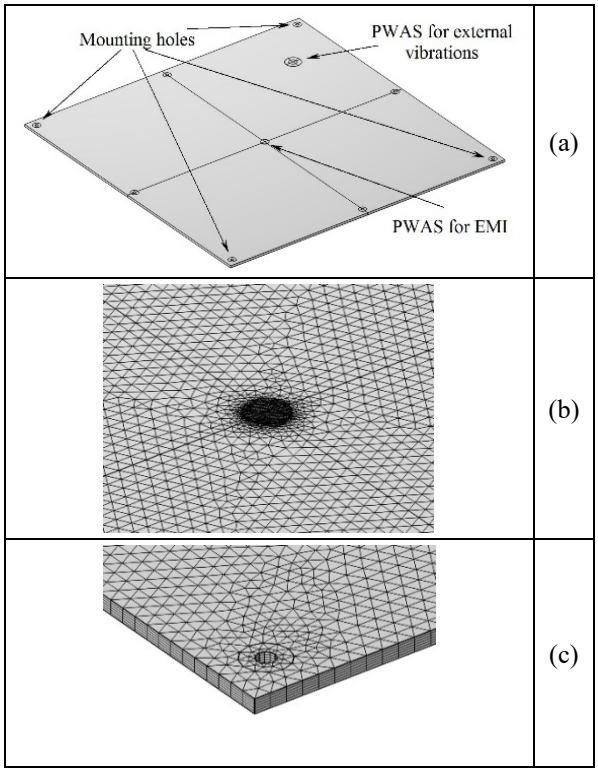

Figure 4. a) Geometry taken in FEM computations; b) Mesh around the PWAS for EMI; c) Mesh of the thickness of the plate.

The geometrical dimensions of the square plates considered in this study, both experimentally and in FEM 3D simulations, are 400mm x 400mm x 3mm.

The PWAS for EMI is positioned at the center of the plate, with dimensions of a diameter of 10mm and a thickness of 0.5mm, with wrap-around electrodes. The PWAS for generating external vibrations is positioned at 65mm from both edges of the plate, with a diameter of 20mm and a thickness of 0.5mm, with wrap-around electrodes (Figure 4.a).

Free boundary conditions for the plate were considered in numerical FEM simulations.

In the 3D FEM numerical simulations, the PWASs with wrap-around electrodes were considered simple PWAS with a ground electrode on the bottom and a terminal electrode on the top, as the wrap-around asymmetry does not influence the computed EMI signature [3]. The mesh used in numerical simulations was considered to be a swept mesh with 6 layers of 0.5mm in thickness for the plate and 2 layers for the PWAS (Figure 4). The faces were meshed with triangle elements, with a maximum size of 2mm, and much finer for both PWAS, with a maximum size of 0.5mm (Figure 4). The analysis was done in the Frequency Domain by sweeping the excitation sinusoidal frequency from 18kHz to 32 kHz, with a 10Hz step. The solution was extracted as the real and imaginary parts of the inverse in-built admittance variable: Y_{11}. Comparisons between numerical simulations and experimental EMI measurements with no vibrations are presented in Figure 5. As can be seen, the experimental and numerically computed EMI signatures are in reasonably good agreement.

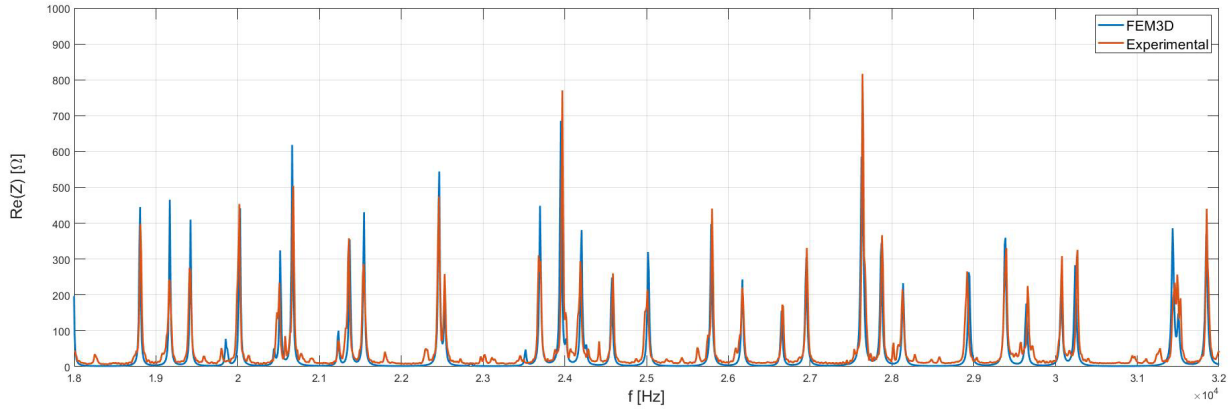

Figure 5. Comparisons of the experimental and numerical FEM3D EMI signature of the considered plate in the absence of vibrations

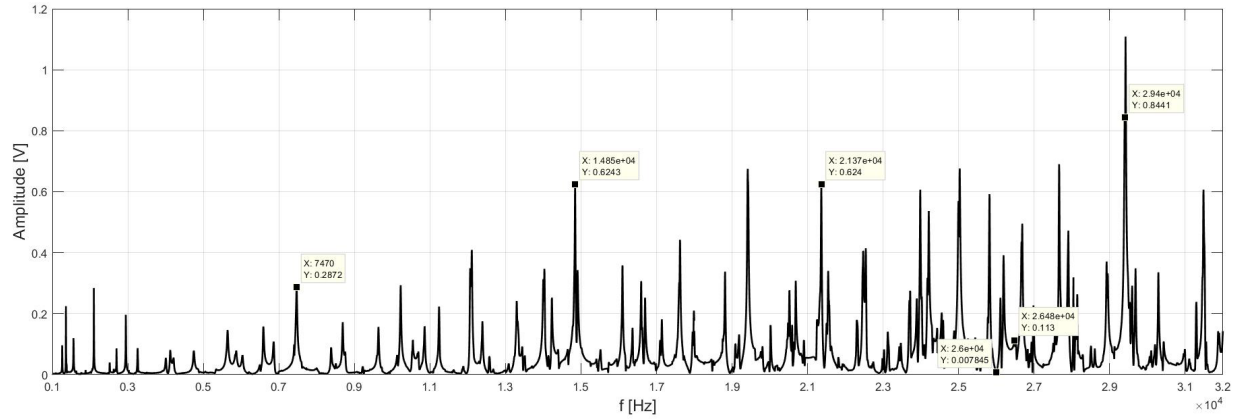

Figure 6. The voltage acquired by the central PWAS in response to vibrations generated by the corner PWAS at a 10V signal at sweeping frequencies from 1kHz to 32kHz

External vibrations induce in the PWASs bonded to the structure an electrical signal that can disrupt the EMI SHM process. Then in a second step an analysis of the external vibrations generated with the corner PWAS over the vibrations existing on the center of the plate that are superposed to the vibrations of the EMI method. By sweeping the frequency of the voltage of 10Vpp applied from the signal generator to the corner PWAS from 1 kHz to 32 kHz, the voltage on the center PWAS was acquired with the oscilloscope, as a relative measurement of the level of vibrations added to the voltage used by the impedance analyzer, as presented in Figure 6. In the next steps, different

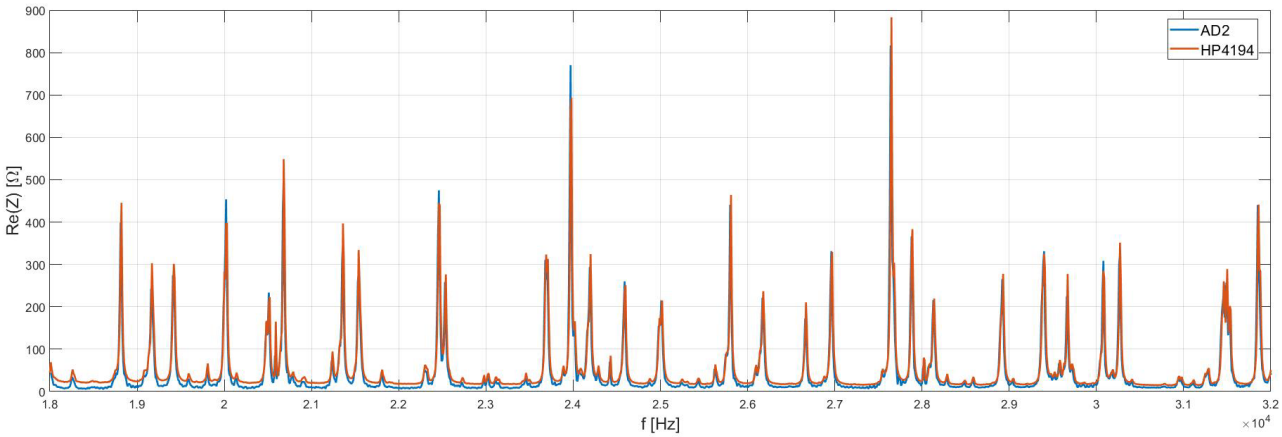

Figure 7. The EMI signature of the considered plate in the absence of vibrations acquired with both AD2 and HP4194 impedance analyzers

vibrations were considered, at frequencies marked on the resonance diagram: 7470 Hz, 14845 Hz, 21370 Hz, 26000 Hz, 26480 Hz, 29400 Hz, taken one at a time or two superposed.

In a third step, a comparison between experimental EMI signatures with both AD2 and HP4194 impedance analyzers has been done, and as can be seen in Figure 7, they are almost identical. The small difference between the AD2 and HP4194 impedance analyzers is in the different types of electronics used. In the next study steps, we considered the measurements done with the AD2 impedance analyzer. To have smaller noise EMI signature measurements, a number of four averages has been taken into consideration.

In the fourth step, comparisons of EMI signatures in cases of different vibrations with the case of no vibrations were done. For these studies, the spectrum used for the EMI analysis was chosen to be between 18 kHz and 32 kHz, with a 10 Hz step. As it is known [1-4], the lower the EMI signature spectrum, the fewer the resonance peaks are, and the easier it is to perform comparisons. And this spectrum is usually used because it is mainly ultrasonic.

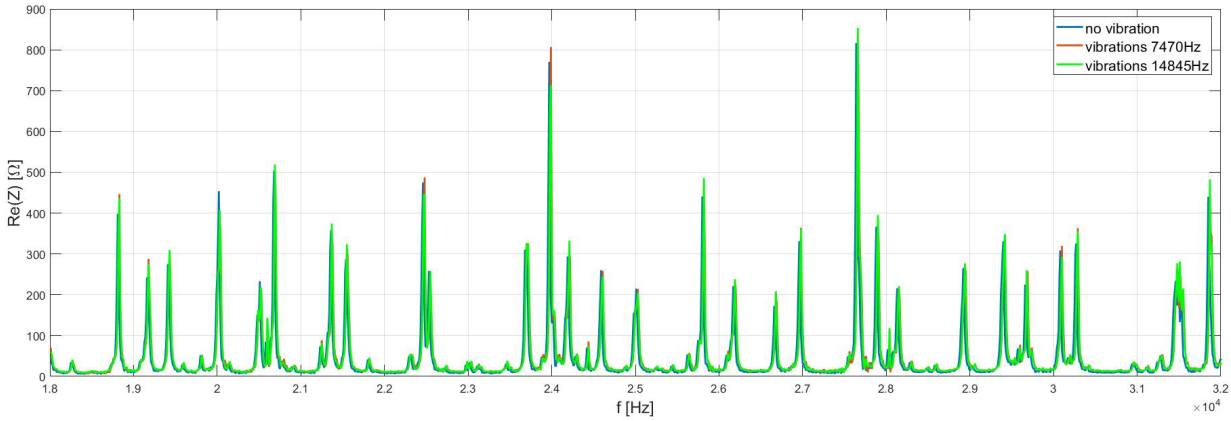

Figure 8. EMI signatures in the cases with no vibrations, and the cases of 7470Hz and 14845Hz vibrations, both out-of-band of the EMI spectrum.

In Figure 8, the EMI signatures in the case with no vibrations are compared with the EMI signatures in the case of vibrations of 7470 Hz and 14845 Hz, both out of the band of the EMI spectrum. It can be seen that these external vibrations, far away from the EMI analysis spectrum, do not influence the EMI signature at all.

In Figure 9, the EMI signatures in the case with no vibrations are compared with EMI signatures in the case of vibrations of 21370 Hz and 26480 Hz, both in-band of the chosen EMI spectrum, measured separately one at a time. As can be seen in Figure 6, the vibration level of 21370 Hz is much higher than the vibration level of 26480 Hz, and so is the error amplitude corresponding to it in the EMI signature. In Figure 10, the EMI signature in the case with no vibrations is compared with the EMI signatures in the case of very weak vibrations of frequency 26000 Hz. It can be seen that in this case, the EMI signature is not influenced.

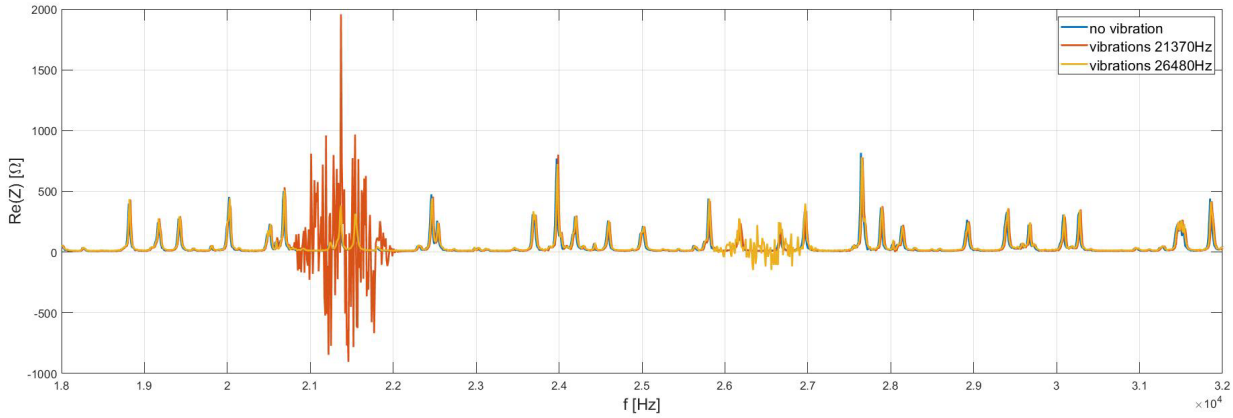

Figure 9. EMI signatures in the cases with no vibrations, and the cases with high-level vibrations at 21370 Hz and low-level vibrations at 26480 Hz, both in-band of the EMI spectrum.

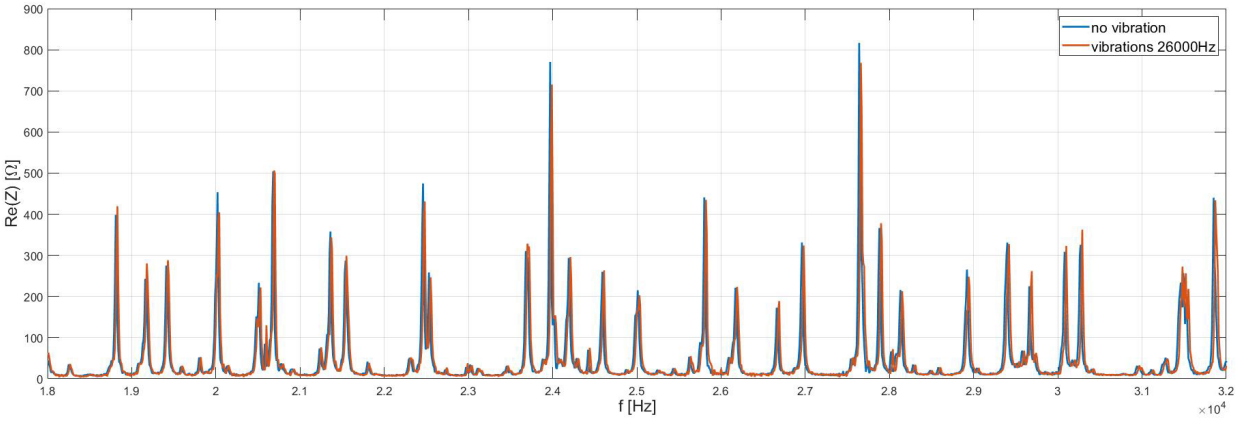

Figure 10. EMI signatures in the cases with no vibrations, and the cases with very weak vibrations at the frequency of 26000 Hz, in-band of the EMI spectrum

In the fifth step, a study of the influence of superposed vibrations at two different frequencies was done. The frequencies considered were 21370 Hz and 29400 Hz (Figure 11), distinct and relatively far apart from each other. As shown in Figure 6, the level of external vibrations induced in the central PWAS is relatively high.

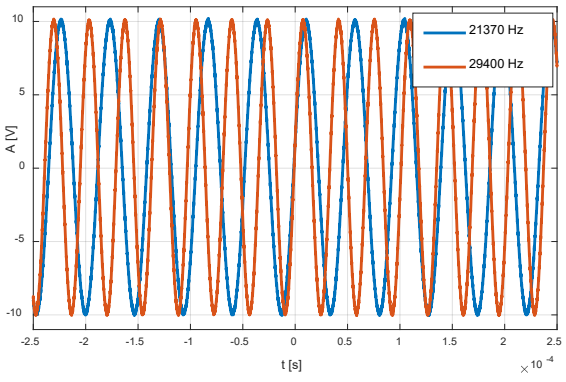

Figure 11. The two signals of frequencies 21370 Hz and 29400 Hz are used separately

The EMI signatures when external vibrations are considered separately, one at a time, and compared with the case of no external vibrations, are plotted in Figure 13. As can be seen, the errors, as in previous cases, are significant. By mixing the two sinusoidal signals of 21370 Hz and 29400 Hz, from Figure 11, on the two channels of the signal generator, a signal plotted in Figure 12 was used to generate composite external vibration by the corner PWAS. The EMI signature of the superposed vibrations compared to the one with no vibrations is plotted in Figure 14. Even if the amplitude of errors when considered superposed (Figure 14) is lower than that considered separately (Figure 13), the spectrum width of the errors is practically the same.

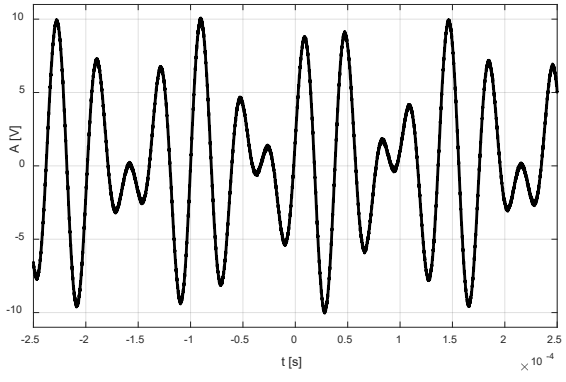

Figure 12. The two signals of frequencies 21370 Hz and 29400 Hz are superposed

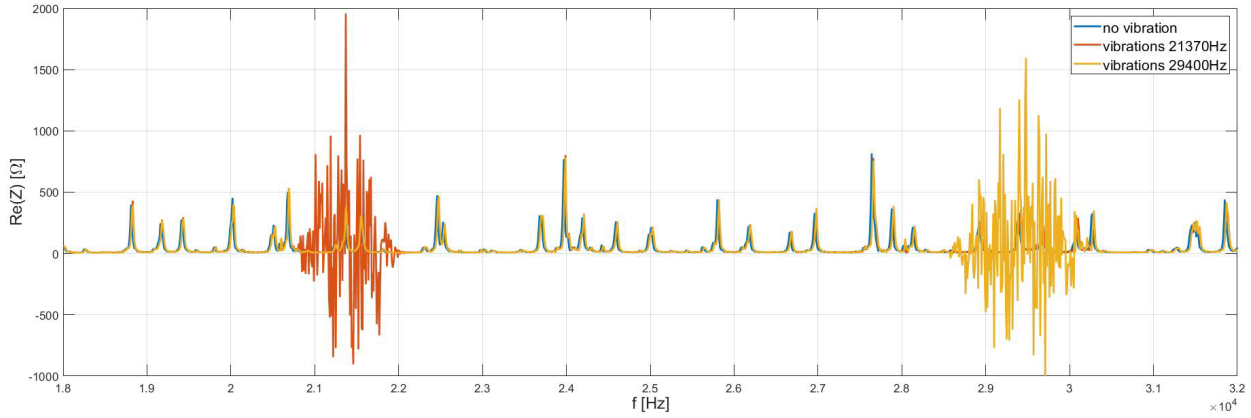

Figure 13. EMI signatures in the case with no vibrations, and the cases of 21370Hz and 29400Hz vibrations, both in-band of the EMI spectrum, taken one at a time.

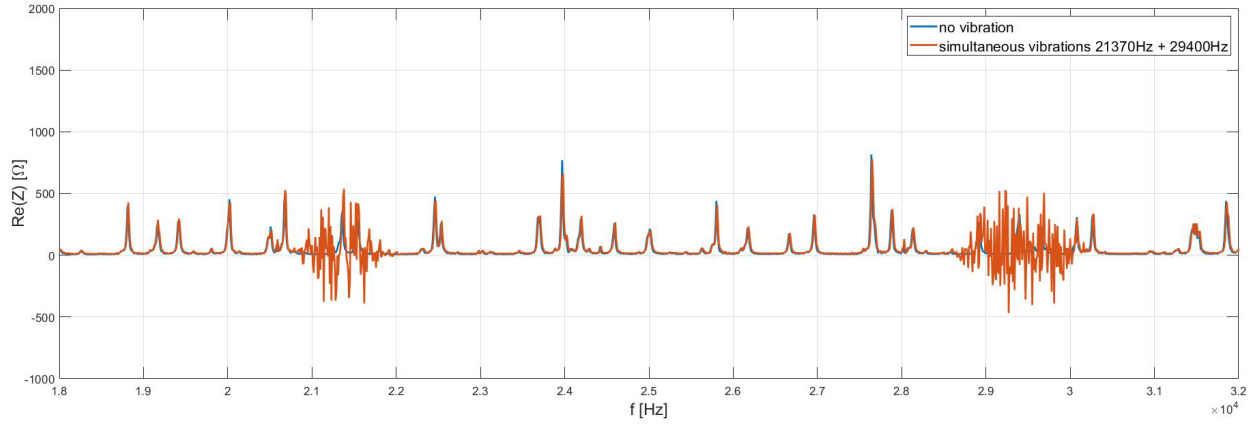

Figure 14. EMI signatures in the case with no vibrations, and the cases of 21370Hz and 29400Hz vibrations, both in-band of the EMI spectrum, superposed.

Another case study analyzes the influence of two levels of external vibrations on the EMI signatures, at the frequency of 29400 Hz, induced by the corner PWAS at 2 Vpp and 10 Vpp by the signal generator. As can be seen in Figure 15, the error levels are proportional to the level of external vibrations of the plate, while the error spectrum width is almost the same.

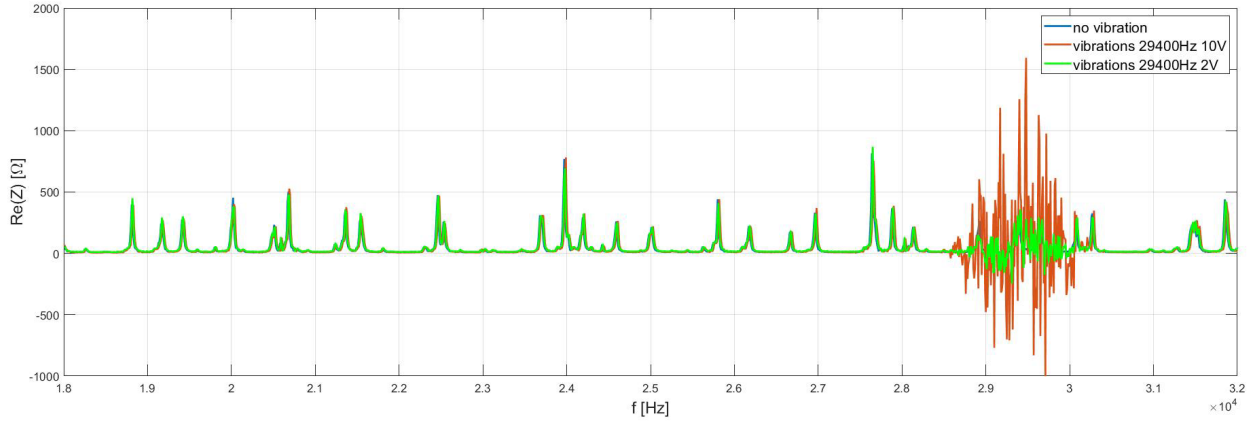

Figure 15. EMI signatures in the case with no vibrations, and the cases of 29400Hz vibrations, with corner PWAS excitation levels of 10Vpp and 2Vpp.

Another comparison was done between the EMI signatures measured with both impedance analyzers, HP4194 and AD2, on the plate subjected to vibrations of 21370Hz, and different numbers of averages, 4 and 64, are presented in Figure 16 and Figure 17. It can be seen that the level and the width spectrum of errors in the EMI signature measured with HP4194 and AD2 impedance analyzers in the presence of vibrations are significantly different for both the averaging taken into account, even if in the

case of the absence of vibrations, as shown in Figure 17, the EMI signature is almost identical. This may be due to different types of electronics incorporated in them, including analog and digital filters, and the algorithms used to deduce the amplitude and phase shift of the signals, which are commercial secrets.

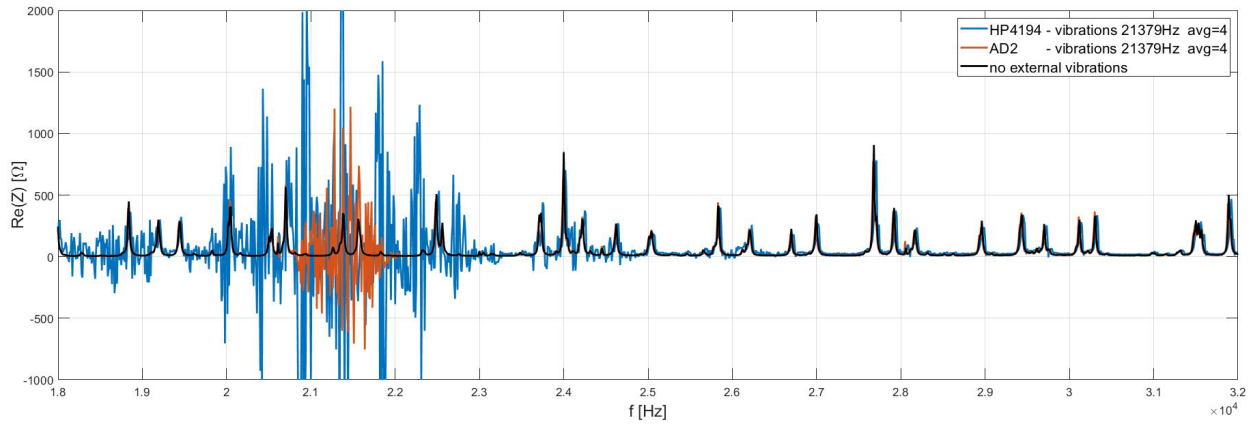

Figure 16. EMI signatures with 4 averages in the cases with no vibrations, and the cases with vibrations of 21370Hz measured with HP4194 and AD2 impedance analyzers

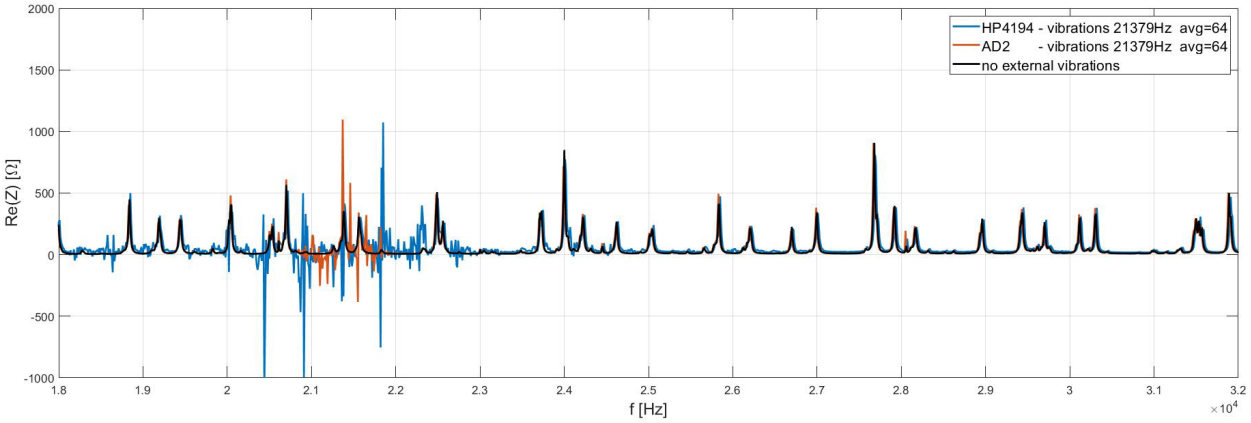

Figure 17. EMI signatures with 64 averages in the cases with no vibrations, and the cases with vibrations of 21370Hz measured with HP4194 and AD2 impedance analyzers

So, theoretical simulations of the EMI method based on the different methods (Integration method (eq.5), Correlation method (eq.7), and Discrete Fourier Transform method (eq.11)) presented in section 2.a, have been applied on theoretical signals reconstructed from the measurements done with the AD2 impedance analyzer. As theoretically studied in [10], these methods are very sensitive to the input signal voltage, sampling rate, and signal-to-noise ratio.

Not knowing all the parameters used by the AD2 impedance analyzer, some key parameters were taken as close as possible in the theoretical simulations of the EMI method in the presence of vibrations.

The amplitude of the input signal was set to 2V, chosen in the software, and the sampling rate of 100Ms/s was used by the data acquisition block of the AD2. As studied in [10], this sampling rate was found to be low, and the errors for all three methods were found to be almost the same for this sampling rate.

The AD2 impedance analyzer provides measured complex values for the voltage (real(V), imag(V)) and current (real(I), imag(I)) for each point of the EMI signature. Based on these values, a mathematical reconstruction of the sinusoidal signals was possible, and a random noise of 1mV was added.

The theoretical EMI signatures calculated by all three methods theoretically studied, in the case without vibration, were found to be the correct ones, identical to the ones measured by the impedance analyzer.

For the EMI signature calculated by all three theoretical methods, Integration (eq.5), Correlation (eq.7), and Discrete Fourier Transform (eq.11) presented in section 2.a, in the case of 21370Hz external vibrations, a voltage level induced in the EMI PWAS by the vibrations generated by the corner PWAS that is superposed to the EMI SHM process, was considered as 0.6V, as the one measured and presented in Figure 6.

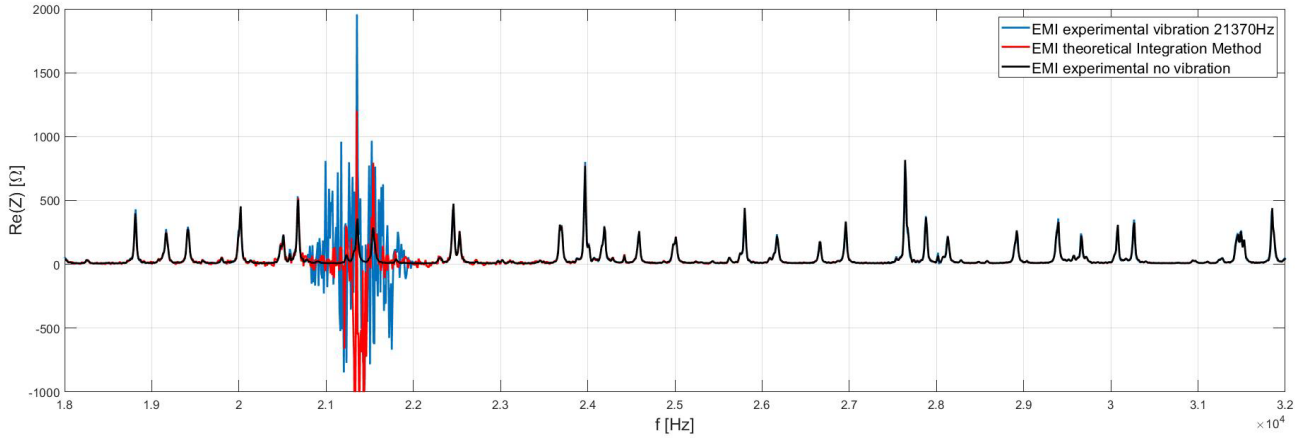

Figure 18. Comparisons of EMI signatures in the cases of experimental with no vibrations, with vibrations of 21370 Hz, and with simulated theoretical results obtained by the Integration method

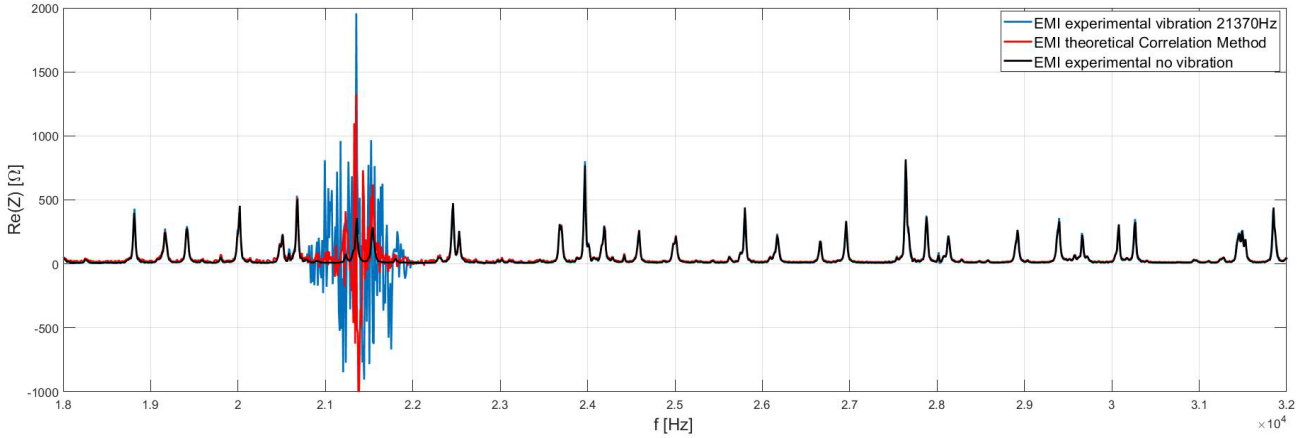

Figure 19. Comparisons of EMI signatures in the cases of experimental with no vibrations, with vibrations of 21370 Hz, and with simulated theoretical results obtained by the Correlation method

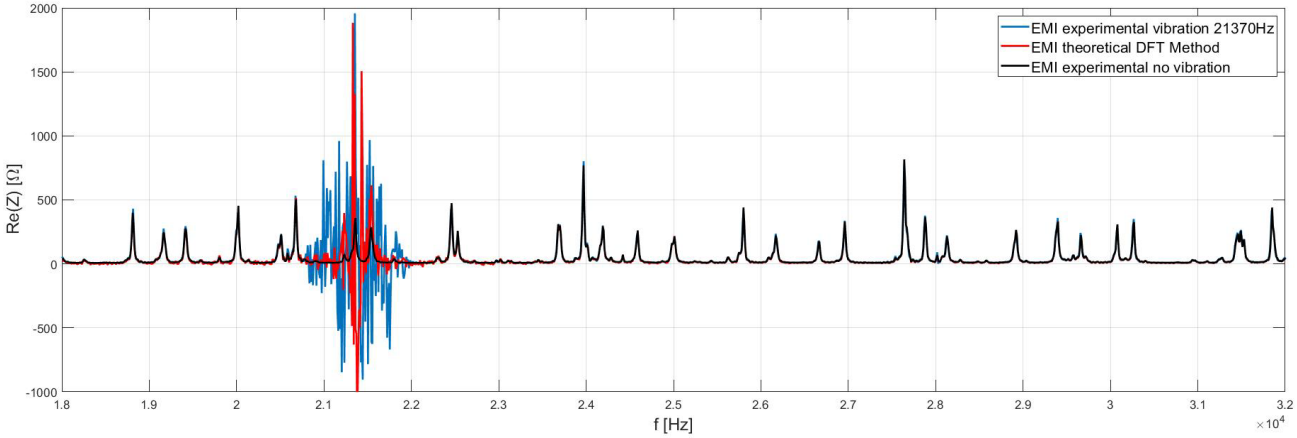

Figure 20. Comparisons of EMI signatures in the cases of experimental with no vibrations, with vibrations of 21370 Hz, and with simulated theoretical results obtained by the Discrete Fourier Transform method.

The theoretical EMI signatures are presented in Figure 18, Figure 19, and Figure 20. It can be seen that they exhibit an error spectrum width around the vibration frequency similar to the ones obtained experimentally. Even if there are differences between the experimental and calculated EMI signatures, these differences are in the error part, which should be avoided anyway. Differences in the error part also appear experimentally when measuring with different types of impedance analyzers, as shown in Figure 16 and Figure 17.

5. CONCLUSIONS

This paper presents a study of the electromechanical impedance method on square plates subjected to small vibrations induced by a second piezoelectric element bonded to the plate by a temporary adhesive, and connected to a signal generator for accurate external frequency vibration control.

It was shown that the temporary adhesive is good enough for this study, giving the same peak position in the EMI signature as in the case of the permanent adhesive, but with lower peak amplitude.

It was shown that external vibrations with a frequency spectrum outside the EMI frequency spectrum do not affect the EMI signature. However, external vibrations with frequencies in the EMI frequency spectrum do affect the EMI signature, not only the specific frequency, but also the surrounding frequencies, in a significant interval width. The levels of external vibrations in the EMI spectrum influence the amplitude of errors, but not the width of the altered EMI signature.

It was shown that the errors in the EMI signature measured by different impedance analyzers are not the same, in the case of vibrations in the EMI spectrum, mainly due to different electronics used.

The theoretical EMI signature calculations confirm the experimental conclusions that vibrations of the structure in the EMI spectrum do affect the EMI signature significantly.

So, when designing an SHM system based on the EMI method, a preliminary study of vibrations existing in the structure must be done, to avoid overlapping the EMI signature chosen spectrum with the one of the external vibrations existing in the structure. In this way, the influence of external vibrations on the EMI signature is completely solved.

ACKNOWLEDGMENTS

This work was supported by a grant from the Ministry of Research, Innovation, and Digitization, CNCS/CCCDI - UEFISCDI, project number PN-IV-P8-8.1-PRE-HE-ORG-2025-0277, within PNCDI IV.

REFERENCES

[1] Giurgiutiu, V., *Structural Health Monitoring with Piezoelectric Wafer Active Sensors,* Elsevier Academic Press, second edition, 2014.

[2] Zagrai, A., Giurgiutiu, V., Electro-mechanical impedance method for crack detection in thin plates, *Journal of Intelligent Material Systems and Structures,* 2001, volume 12, issue 10, pp. 709-718
DOI: 10.1177/104538901320560355.

[3] Rugina, C., Enciu, D., Tudose, M., Numerical and experimental study of circular disc electromechanical impedance spectroscopy signature changes due to structural damage and sensor degradation, *Structural Health Monitoring*, 2015, volume **14**, issue *6*, pp. 663–681,
DOI: 10.1177/1475921715610927.

[4] Rugina, C., Toader, A., Giurgiutiu, V., Ursu, I., The electromechanical impedance method for structural health monitoring of thin circular plates, *Proceedings of the Romanian Academy, Series A*, 2014, volume **15**, no. *3*, pp. 272–282.

[5] Enciu, D., Ursu, I., Toader, A., New results concerning structural health monitoring technology qualification for transfer to space vehicles, *Structural Control and Health Monitoring*, 2017, ISSN: 1545-2263, DOI: 10.1002/stc. 1992.

[6] Kamas, T., Giurgiutiu, V., Lin, B., E/M impedance modeling and experimentation for the piezoelectric wafer active sensor, *Smart Materials and Structures*, 2015, volume 24, issue 11, pp. 5040-5053, DOI: 10.1088/0964-1726/24/11/115040.

[7] Na, W.S., Baek, J., A Review of the Piezoelectric Electromechanical Impedance Based Structural Health Monitoring Technique for Engineering Structures, *Sensors*, 2018, volume 18, issue 5, article .no. 1307; DOI:10.3390/s18051307.

[8] Yang Y., Miao A., Effect of External Vibration on PZT Impedance Signature, *Sensor*, 2008, Vol. 8, Issue 11, pp. 6846-6859,
DOI:10.3390/s8116846.

[9] Campeiro, L.M., Da Silveira, R.Z.M., Baptista F.G., Impedance-based damage detection under noise and vibration effects, *Structural Health Monitoring*, 2018, volume 17, issue *3*, pp. 654-667,
DOI: 10.1177/1475921717715240

[10] Giurgiutiu, V., Xu, B., Development of a Field-Portable Small-Size Impedance Analyzer for Structural Health Monitoring using the electromechanical Impedance Technique, *Proc. of SPIE: Smart Structures and Materials: Sensors and Smart Structures Technologies for Civil, Mechanical, and Aerospace Systems*, Vol. 5391, pp. 774-785, 2004,
DOI: 10.1117/12.541343

[11] *** IEEE std 176-1987 - *Standard on Piezoelectricity,* DOI:10.1109/IEEESTD.1988.79638.